◆ Human Brain Mapping 12:180–192(2001) ◆

Three-Dimensional Integration of Brain Anatomy and Function to Facilitate Intraoperative Navigation Around the Sensorimotor Strip

Jyrki P. Mäkelä,[1,5]* Erika Kirveskari,[1] Mika Seppä,[1] Matti Hämäläinen,[1] Nina Forss,[1] Sari Avikainen,[1] Oili Salonen,[2] Stephan Salenius,[1] Tero Kovala,[5] Tarja Randell,[3] Juha Jääskeläinen,[4] and Riitta Hari[1,5]

[1]*Brain Research Unit, Low Temperature Laboratory, Helsinki University of Technology, Espoo, Finland*
[2]*Department of Radiology, Helsinki University Central Hospital, Helsinki, Finland*
[3]*Department of Anesthesiology, Helsinki University Central Hospital, Helsinki, Finland*
[4]*Department of Neurosurgery, Helsinki University Central Hospital, Helsinki, Finland*
[5]*Department of Neurology and Clinical Neurophysiology, Helsinki University Central Hospital, Helsinki, Finland*

Abstract: We studied 12 patients with brain tumors in the vicinity of the sensorimotor region to provide a preoperative three-dimensional visualization of the functional anatomy of the rolandic cortex. We also evaluated the role of cortex-muscle coherence analysis and anatomical landmarks in identifying the sensorimotor cortex. The functional landmarks were based on neuromagnetic recordings with a whole-scalp magnetometer, coregistred with magnetic resonance images. Evoked fields to median and tibial nerve and lip stimuli were recorded to identify hand, foot and face representations in the somatosensory cortex. Oscillatory cortical activity, coherent with surface electromyogram during isometric muscle contraction, was analyzed to reveal the hand and foot representations in the precentral motor cortex. The central sulcus was identified also by available anatomical landmarks. The source locations, calculated from the neuromagnetic data, were displayed on 3-D surface reconstructions of the individual brains, including the veins. The preoperative data were verified during awake craniotomy by cortical stimulation in 7 patients and by cortical somatosensory evoked potentials in 5 patients. Sources of somatosensory evoked fields identified correctly the postcentral gyrus in all patients. Useful corroborative information was obtained from anatomical landmarks in 11 patients and from cortex-muscle correlograms in 8 patients. The preoperative visualization of the functional anatomy of the sensorimotor strip assisted in designing the operational strategy, facilitated orientation of the neurosurgeon during the operation, and speeded up the selection of sites for intraoperative stimulation or mapping, thereby helping to prevent damage of eloquent brain areas during surgery. *Hum. Brain Mapping 12:180–192, 2001.*

Key words: central sulcus; magnetoencephalography; magnetic resonace images; MRI venography; somatomotor strip; somatomotor evoked responses; 3-D imaging; tumor resection

INTRODUCTION

Tumors, vascular malformations, and previous operations may deform brain anatomy so that it is impossible to identify, e.g., primary motor cortex from

*Correspondence to: J. P. Mäkelä, Brain Research Unit, Low Temperature Laboratory, Helsinki University of Technology, P.O. Box 2200, 02015, Espoo, Finland.

Received for publication 8 November 1999; accepted 18 December 2000

preoperative magnetic resonance (MR) images, or from anatomic landmarks during surgery. Grade II-IV gliomas infiltrate the brain diffusely; their surgery is a tradeoff between an extensive enough resection, and the danger of damage to adjacent eloquent brain areas. The situation is complicated by cortical reorganization due to tumor, which may alter somatosensory representations [Wunderlich et al., 1998]. Furthermore, functional cortex may intermingle with low-grade glioma tissue [Skirboll et al., 1996]. Consequently, glioma surgery benefits from information about the functional anatomy of the brain areas in the tumor region.

Source locations of magnetoencephalographic (MEG) signals, displayed on three-dimensional MR images, including the blood vessels on the brain surface, aid in pinpointing functionally irretrievable areas before and during neurosurgery [Gallen et al., 1993; Kamada et al., 1993; Gallen et al., 1995]. Presurgical MEG studies may reveal dislocation of functional areas to unexpected directions and thus prevent their inadvertent damage. The recordings may also encourage operations on tumors in eloquent brain areas when the functional regions are pushed aside but remain unaffected by the tumor tissue. MEG is more practical in evaluation of sources of brain activity than the more widely used EEG. Local changes in conductivity due to different tissues or, for example burr holes from the previous operations do not significantly affect magnetic fields, whereas electric potentials are clearly distorted.

The sources of the somatosensory evoked fields (SEFs) to electric stimulation of peripheral nerves (for a recent review, see Hari and Forss, 1999) accurately identify the posterior wall of the central sulcus [Sutherling et al., 1988]. Sensory deficits following lesion of the somatosensory cortex may render a limb largely useless. However, the primary motor cortex in the anterior wall of the sulcus has to be particularly well protected during operations to prevent postoperative paresis. Recordings of movement-related fields have been used to locate the motor cortex (e.g., Rezai et al., 1996). In healthy subjects, fast and direct localization of motor strip has been shown to be feasible also by using correlograms between cortical spontaneous MEG and surface electromyograms (EMGs). The 15-30 Hz rhythmic activity of the motor cortex is coherent with the EMG of muscles during isometric contraction [Conway et al., 1995; Salenius et al., 1997; Hari and Salenius, 1999], indicating that rhythmic cortical activity induces a similar rhythmicity in the descending motor commands. The generation sites of cortical MEG signals coherent with the surface EMG from the activated muscles indicate crude somatotopical organization in the primary motor cortex [Salenius, et al., 1997]. Motor cortex origin of the coherent signals is also supported by direct recordings from the monkey motor cortex [Baker et al., 1997]. Our study is the first description of presurgical motor cortex identification applying this method.

To improve visualization of the functional brain anatomy in the sensorimotor strip of neurosurgical patients by SEFs, we compared the sources of the MEG signals coherent with EMG with data from intraoperative cortical stimulation and recordings to confirm their motor cortex origin, and assessed the value of this new tool in identifying the motor cortex in patients with brain tumors. Furthermore, we identified the central sulcus by anatomical MRI landmarks, available when the tumor did not cause significant swelling and deformation. Our aim was to locate the sensorimotor strip as reliably as possible by combining information from different methods.

MATERIALS AND METHODS

Patients

Twelve patients (27–60 yrs) were studied; five had primary, and four recurrent GII or GIII gliomas, one had a metastatic neurofibrosarcoma, one a hemangioma, and one an arteriovenous malformation in the vicinity of the sensorimotor strip (Table I). The adjacent somatosensory and motor cortical areas were identified with MEG. Eleven of the twelve patients were operated on with awake craniotomy; one patient had a stroke a day before the planned operation.

Recording and data analysis

The MEG recordings were carried out in a magnetically shielded room with a whole-scalp SQUID (Superconducting QUantum Interference Device) magnetometer [Neuromag 122^{TM}; Ahonen et al., 1993]. The 122 sensor units of the device are arranged in a helmet-shaped array and measure the two orthogonal tangential derivatives of the magnetic field component normal to the helmet surface at 61 measurement sites.

Somatosensory evoked fields were elicited by electric stimulation (0.2 ms; intensity above the motor threshold; interstimulus interval, ISI, 0.5 s) of the median nerve (MN) at the wrist and the posterior tibial nerve (TN) at the ankle, and by 250-Hz vibratory stimulation (4 ms; ISI 0.5 s) of the upper lip (LIP). Auditory evoked fields (AEFs) were elicited by tones (1 kHz; 50 ms; ISI 1 s) delivered alternately to both ears. For cortex-muscle correlograms, a 4-min period

TABLE I. Patients with tumors in the vicinity of the somatomotor strip. Pr.O. indicates previous operation

Pat	Sex/age	Histology	Pr.O	Location	Symptoms	Postop. symptoms < 1 week	Postop. symptoms > 1 month
1	F/19	neurofibrosarcoma	−	r. frontoparietal	focal seizures	sensorimotor paresis of l. lower limb	l. ankle weakness
2	M/59	astrocytoma GII	−	l. frontoparietal	weakness of r. limbs	transient r. hemiparesis, dysphasia	weakness of r. lower limb
3	F/37	AV-malformation	−	l. frontoparietal	1 GM seizure, weakness and sensory defect of r. lower limb	r. sensorimotor hemiparesis	none
4	F/33	oligodendroglioma GII	−	l. frontoparietal	epilepsy	transient dysexecutive syndrome	none
5	M/28	astrocytoma GII	+	r. frontoparietal	epilepsy, sensory defect of l. foot	transient l. upper limb ataxia	clumsiness & sensory defect of left ankle and foot
6	M/57	astrocytoma GII	−	r. frontoparietal	focal seizures, weakness of l. lower limb	not operated	
7	F/49	oligodendroglioma GII	+	l. posteriofrontal	focal seizures	transient r. hemiparesis, dysphasia	none
8	M/47	oligoastrocytoma GII	+	l. parietal	sensorimotor symptoms of r. upper body, dysphasia	as earlier	sensory defect of r. upper limb, dysphasia (less pronounced)
9	F/52	oligoastrocytoma GII	−	l. parietal	sensorimotor defect of r. limbs	weakness and ataxia of r. limbs, occasional dysphasia	none
10	F/54	hemangioma	−	r. frontoparietal	1 seizure	none	none
11	M/43	oligoastrocytoma GIII	+	l. temporal	r. hemiparesis, dysphasia, amnesia, epilepsy, decreased cogn. performance	transient worsening of hemiparesis, desorientation	weakness of r. lower limb, worsening of dysphasia, further decreased cogn. performance
12	F/51	astrocytoma GIII	−	r. frontal	clumsiness of l. foot l. ankle foot drop	increase of l. foot weakness	corresponds to preoperative condition

of spontaneous MEG activity was collected during isometric muscle contraction; simultaneous surface EMG was recorded from extensor carpi radialis muscle in the forearm and tibialis anterior muscle in the shin.

During the recordings, the patient was seated under the helmet-shaped neuromagnetometer with the head leaning against its bottom. The exact location of the patient's head with respect to the sensors was determined by measuring the magnetic field produced by small currents delivered to four coils attached to the scalp. The locations of the coils with respect to the nasion and periauricular points were determined with a 3-D digitizer; this information was used to align the MEG and MRI coordinate systems. Before digitization, the fiduciary points were marked on the skin, and the nasion and the auricular folds were photographed with a digital camera. The photographs were used during data analysis for more precise identification of the fiduciary points from the MR images.

The recording passband was 0.03–320 Hz (3 dB points, high-pass roll-off 35 dB/decade, lowpass over 80 dB/decade) for MN and TN stimulations; sampling rate was 987 Hz. For LIP-SEFs, the corresponding values were 0.03–100 Hz and 397 Hz, and for AEFs 0.03–90 Hz and 297 Hz. The 500-ms analysis period included a 100-ms pre-stimulus baseline. About 120 responses were averaged for MN-SEFs and AEFs, and about 500 for TN-SEFs and LIP-SEFs; two subaverages were calculated from alternate responses to confirm the response replicability. The vertical electro-oculogram (EOG) was recorded simultaneously and epochs in which the EOG activity exceeded ± 150 μV were rejected from the averages. The spontaneous MEG activity was recorded with a 0.03–190 Hz passband and a 597 Hz sampling rate; EMG was collected with 3–100 Hz passband.

The averaged responses were digitally low-pass filtered at 190 Hz (SEFs) or at 40 Hz (AEFs). The head was modelled as a spherical volume conductor, matched to the local curvature of the inner skull in the region of intrest. Spherical head model has been shown to be as accurate over the somatosensory and auditory areas as the realistic head model [Hämäläinen and Sarvas, 1989]. Sources of maximum deflections were modelled as equivalent current dipoles (ECDs), found by a least-squares fit to signals recorded by a subset of 18 to 24 channels surrounding the maximum signals over each hemisphere. Only ECDs explaining at least 80% of the field variance were accepted; the mean $\pm$ SD value was 93 $\pm$ 4% for MN and 90 $\pm$ 6 % for TN sources. The MN source was searched during 18-33 ms and the TN source during 39-59 ms after the stimulus onset; the corresponding range was 40–80 ms for LIP-SEFs and 80–130 ms for AEFs.

MEG-EMG cross- and coherence spectra were computed [Rosenberg et al., 1989] with a frequency resolution of 1.2 Hz. Cross-correlograms were obtained by an inverse Fourier transform of the coherence. Cortical sources for activity coherent with EMG were identified at the strongest cross-correlogram peaks and modeled by ECDs.

The MR images (1.5 T Siemens Vision system) were acquired using regular T1-weighted MPRAGE sequence for head images and gadolinium-enhanced MPRAGE sequence for visualizing the venous system and tumor enhancement. The slices, spaced by 1 mm, were acquired in the sagittal orientation. The brain was segmented from the regular T1-weighted MRI data with semiautomatic software developed in our laboratory; the program offers a comprehensive set of 2-D and 3-D image processing operations, including thresholding and region growing. With this method, an experienced user can accomplish the brain segmentation in less than 10 minutes.

To depict the veins on the brain surface, the contrast-enhanced MR images were segmented along the inner surface of the skull, but the program had problems in finding the border between the dura and the skull. Consequently, the 3-D operators were used to obtain a rough estimate of the inner surface of the skull, and interactive image editing tools available in the software were then applied manually to extract the veins. This procedure took 3–4 h per patient.

We also evaluated MR angiography (MRA) images in the vein visualization. MRA was a phase -contrast angiography sequence. The following parameters were used: TR 83 ms/TE 9 ms /flip angle 11 degrees, matrix 192×256, single aquisition and a 250 field of view yielded an in-plain pixel size of 1.04×0.78 mm^2. Transaxial slab, 34 mm thick, with 16 partitions and resulting in section thickness of 2.12 mm was used. The time of aquisition was 4 min 17 s. The segmentation of the MRA images was easily achieved by a simple thresholding operation and then confining the volume to the inside of the skull as determined from the regular T1-weighted images. This volume selection removed the blood vessels extending into the skull and the scalp. The co-registration of MRA data with the regular T1-weighted images was problematic, because these two data sets did not share any common visible anatomical landmarks. Thus, we gathered the images sequentially and used the MR device's coordinate system to align the image sets. For this procedure, we had to assume that the head did

TABLE II. Useful findings (+) in the affected hemisphere for localization of the central sulcus

Patient	MN-SEF	TN-SEF	COHu	COHl	Knob	Width	c.s.	SEP	Stimulation	Difference (mm)
1	+	+	+	+	+	+	+	na	na	−
2	+	+	−	−	+	u	+	na	na	−
3	+	+	−	+	+	+	+	na	na	−
4	+	+	−	−	+	+	+	na	hand & lip motor	−
5	+	−	−	−	+	+	−	na	limbs motor	−
6	+	−	+	−	+	+	+	na	(not operated)	−
7	+	+	−	−	+	+	+	na	hand & lip & leg motor, speech	−
8	+	+	+	+	+	−	+	+	speech	MN-SEF/SEP 6
9	+	+	+	+	+	+	+	+	hand motor & sensory, speech fingers (2–5)	MN-SEF/SEP 9 MN-SEF/sSTIMfin 8 MN-SEF/SEP 7
10	+	+	−	−	+	−	+	+	motor & sensory, lip sensory	MN SEF/sSTIMfin 8 LIP-SEF/sSTIMlip 8
11	+	+	+	+	+	+	+	+	hand motor	MN-SEF/SEP 18
12	+	+	+	−	−	+	−	+	limbs motor	MN-SEF/SEP 9 COHu/mSTIMfin 6

MN-SEF: SEF to median nerve stimulation.
TN-SEF: SEF to posterior tibial nerve stimulation.
COHu: Coherent MEG-EMG activity (upper limb).
COHl: Coherent MEG-EMG activity (lower limb).
Knob: knob in the hand area detectable (+).
Width: width of precentral gyrus: larger (+), equal or smaller than postcentral gyrus (−), undefinable (u) because of tumor mass.
c.s.: central sulcus detectable (+)/not detectable (−) just anterior to the ramus posterior of the cingulate sulcus in the mesial surface of the hemisphere.
SEP: intraoperative SEP to median nerve stimulation; SEP not available (na).
Stimulation: effect of intracortical stimulation; stimulation not available (na).
Difference: Separation of estimated and intraoperative localization; sSTIMfin, sSTIMlip sites eliciting finger and lip sensations in intracortical stimulation; mSTIMfin site eliciting finger movements in intracortical stimulation.

not move between the two acquisitions and that the possible distortion of the real space in the images was identical. A detailed inspection of the overlaid images occasionally showed a misalignment of a few millimeters. Therefore, only the contrast-enhanced MR, not MRA images were used for the vein visualization.

The software for the visualization of the segmented images was developed in our laboratory. This program uses the ray-tracing method to model the virtual path of light. The texture or the surface color of the segmented volume is achieved by integrating the intersecting ray a given number of voxels into the volume. The relative positions of the intersection point and light sources and the local surface normal then determine the lighting factors. The MEG source locations were visualized as colored dots on top of the ray-traced raster images. The ECDs were generally located at some depth within a sulcus, and the ambiguity caused by parallax distortion in projecting them to the brain surface was solved by identifying the appropriate sulcus from traditional MR images in three planes and following it onto the cortical surface.

The anatomical identification of the motor cortex was based on the omega-shaped knob in the hand area [Yousry et al., 1997], and morphological identification of the central sulcus on the basis of its continuation from the mesial surface, just anterior to the well identifiable posterior ramus of the cingulate sulcus [Berger et al., 1990]. We also tested an old notion of broader precentral motor than postcentral somatosensory gyrus at the vertex (Prof. K. Zilles, personal communication) by measuring the width of precentral and postcentral gyrus 3 mm lateral from the medial border of the hemispheric cortex in the longitudinal fissure.

Procedures during awake craniotomy

The patients were preoperatively acquainted with the intraoperative testing of motor and speech functions, and the neurosurgeon and the neuroanaesthesi-

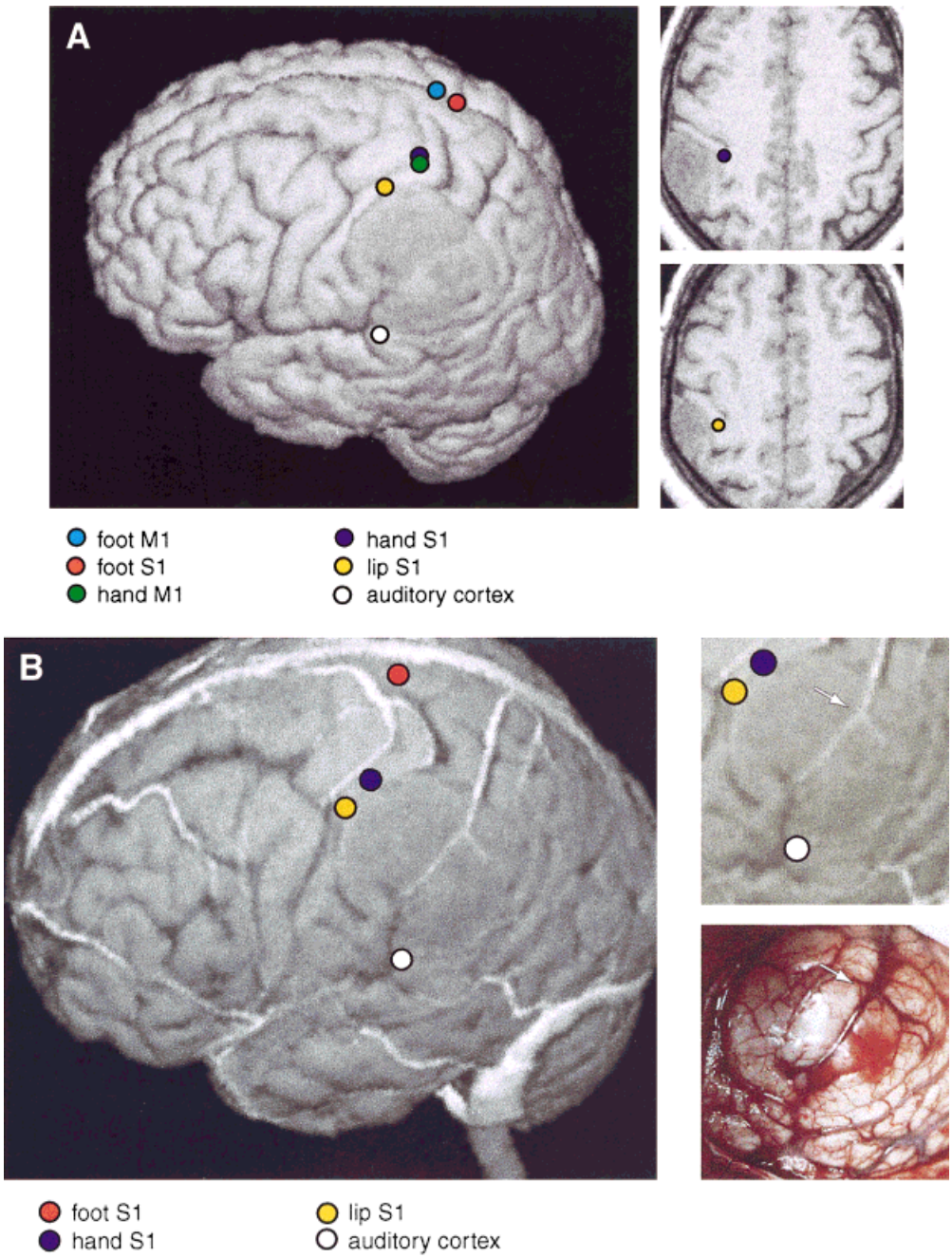

Figure 1.

A:Left: 3-D surface rendering of the brain of Patient 9. The left parietal GII oligoastrocytoma is readily identifiable. The equivalent current sources of responses to MN-SEFs, TN-SEFs, LIP-SEFs and AEFs, and MEG-EMG coherences for right wrist and ankle extensions are displayed on the surface. Right: Sources of SEFs to median nerve and lip stimulation, displayed on two horizontal MRI sections. Note the distortion of functional cortical anatomy by the slowly growing tumor. **B.** Left: 3-D surface rendering of the brain of Patient 9, including cortical veins and sources of SEFs and AEFs. Right, above: Enlarged section of 3-D MRI surface rendering. Right, below: Corresponding brain surface during surgery. The veins are readily identifiable and allow both the localization of the somatosensory cortex (left) and the tumor area (right, below) (vein bifurcation over the tumor is marked with an arrow). **C.** Left: Postoperative surface rendering of Patient 9. Sources of MEG-EMG coherences for right wrist and ankle extensions, and MN-SEFs, TN-SEFs, LIP-SEFs and AEFs, are displayed on the surface. Right: Sagittal and coronal sections of the postoperative MRIs, with sources of median nerve SEFs and hand MEG-EMG coherence.

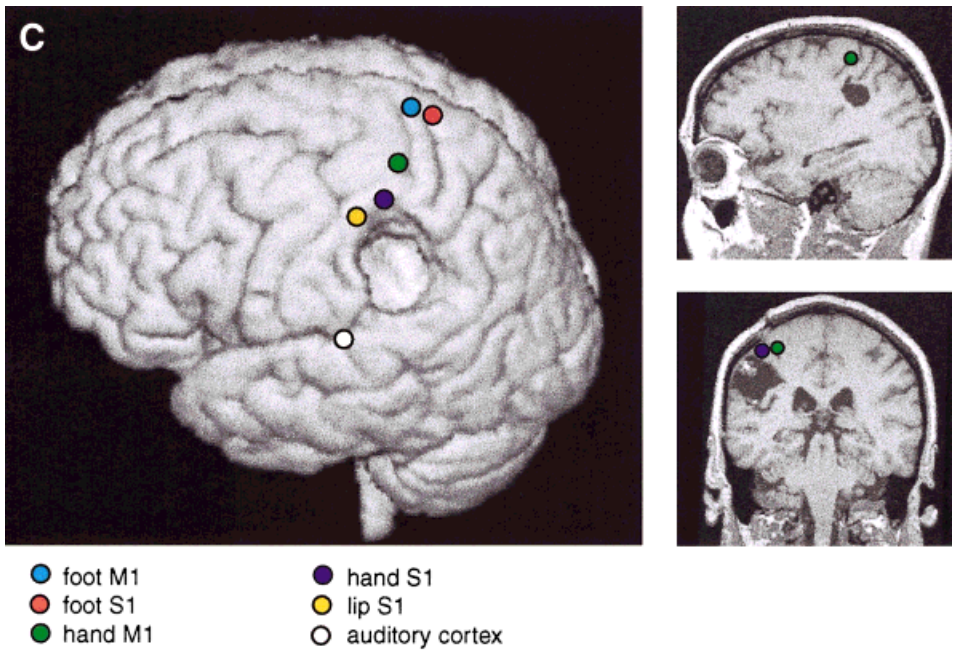

Figure 1.

ologist explained thoroughly the course of the surgery, performed under local anesthesia. The patients were premedicated with peroral diazepam, ondansetron and ranitidine. During surgery, the head was fixed in an ordinary head frame, fixed to the operation table. A comfortable position, and visual contact to the neuropsychologist and the speech therapist were then ascertained. The patient was sedated by propofol infusion to be drowsy during opening and closure of the skull, but was maintained alert during cortical stimulation and tumor removal. Functional cortical areas around and over the tumor were identified by comparing the exposed cortex with the MEG sources and cortical veins superimposed on the 3-D MRIs of the cortex. The propofol infusion was then discontinued and the motor and somatosensory cortices were identified using unipolar cortical stimulation and grid corticography. Subsequently, the tumor tissue was removed under the operating microscope.

Intraoperative recordings

Intraoperatively, cortical somatosensory evoked potentials (SEPs) were recorded from five patients (8-channel Viking IV recorder; Nicolet^{TM}; Table II). Median nerve was stimulated at the wrist with 0.2-ms electric pulses once every 250 ms, with stimulus intensities slightly exceeding the motor threshold. The responses were recorded from two first rows of a 4 × 5 electrode grid (PMT Inc., Minnesota, U.S.A), consisting of 6.5-mm diameter silver-silver chloride electrodes separated by 3 mm. The grid was placed over the central sulcus hand region. A needle in the temporal muscle was used as reference, and the ground electrode was proximal to the stimulation electrode in the stimulated limb. Phase reversal of the 20–25 ms response was used to indicate the location of the central sulcus [Wood et al., 1988]. The recording grid, with 8 active electrodes, did not allow exact definition of the course of the polarity reversal line of the SEPs.

The cortical area around and over the tumor region was mapped for motor, sensory and speech function in seven patients, using 50-Hz 0.2-ms 9–18 mA unipolar electric pulses. The diameter of the disk-shaped tip of the probe was 4 mm. The stimulation was performed under 1 cm × 0.7 cm paper tags; the optimum response site was not searched. The cortical surface, location of stimulation sites, and the SEP grid position were photographed for comparison with preoperative findings.

To provide a rough estimate of the location accuracy of the SEF sources, the sensory cortical areas identified by intraoperative cortical stimulation and the sites of cortical electrodes displaying maximum negative SEP deflections in 20–25 ms range were superimposed on the surface of the individual 3-D MRI reconstructions. The MEG sources were projected to the nearest brain surface. The distance between the identified stimula-

tion points or electrode sites and the SEF sources was then measured.

RESULTS

Figure 1 illustrates data from Patient 9 with an anterior parietal tumor, 5 cm in diameter. SEF recordings (MN, TN, LIP) identified the somatosensory cortex, which was dislocated anteriorly by the tumor (Fig. 1A). The MEG-EMG correlogram confirmed the location of the central sulcus. The sources were close to those of the median nerve SEFs. During the awake craniotomy, the somatosensory cortex and the tumor were readily identified by the veins presented on the 3-D MRI surface rendering (Fig. 1B). Cortical stimulation of the regions predicted by SEF sources produced parestesia and sensations in the right hand and corner of the mouth. Cortical SEPs inverted in polarity along the course of the estimated central sulcus. Grade III oligoastrocytoma was microsurgically removed with no permanent postoperative paresis or speech disorders (Table I). The postoperative MRI showed a near-total tumor removal, and the source of the MEG activity coherent with EMG was now clearly separable from the SEF source, corresponding to motor cortex localization by anatomical landmarks (Fig. 1C).

Figure 2 shows data from a patient with a cavernous hemangioma in the right lower parietal lobe. SEFs (MN, TN, LIP) identified the somatosensory cortex. The hemangioma was located beneath the source of the MN-SEFs and posterior to the source of the 100-ms AEF. Properly sectioned 3-D MRIs showed that the upper branch of the end of the sylvian fissure led directly to the tumor (Fig. 2A).

During awake craniotomy, the cortex identified by the sources of the AEFs and SEFs was exposed, and the gyral and vascular patterns were readily identifiable. Cortical stimulation elicited finger and lip sensations from locations corresponding to the SEF sources; in addition, finger movements were elicited from precentral gyrus from the level of the MN-SEF sources. Cortical SEPs confirmed the location of the central sulcus (Fig. 2B). The hemangioma was removed by opening the branch of the sylvian fissure, without any postoperative deficits.

Figure 3 depicts findings from patient 12 with a GIII astrocytoma in the right frontal lobe. The MEG-EMG coherence during wrist extension was strongest in the precentral gyrus whereas ankle extension did not produce reliable MEG-EMG coherence. The central sulcus was also identified by SEFs elicited by median and tibial nerve stimulations. Intraoperative stimulation of the source site of maximum coherence elicited finger movements, and stimulation of the foot motor area, estimated from the sources of tibial SEFs, elicited foot movements.

Table II summarizes the value of different methods in locating the central sulcus. The preoperative identification, using all available landmarks, generally agreed with intracortical stimulation and SEP data. The mean distance between the SEF source and the SEP electrode picking up the maximum 20-ms response was 10 mm (range 5–18 mm; cf. Table II). In one patient, the distance was 18 mm along the postcentral gyrus, and thus did not affect the identification of the central sulcus. In other subjects, the difference varied between 5-10 mm. The mean distance between the site producing sensory response in cortical stimulation and SEF source was 8 mm. The intraoperative stimulation findings deviated from preoperative localization only in Patient 5 who had a recurrent parasagittal GII astrocytoma, and in whom TN-SEFs and MEG-EMG coherences were not detected. Cortical stimulation indicated that motor cortex was anterior to tumor, not posterior to it as expected. Retrospective analysis based on MN-SEFs and on the omega-shaped knob observed in MRI agreed with this localization as well (Fig. 4). In Patient 1, the TN-SEF source was paradoxically projected inside a solid metastatic neurofibrosarcoma, suggesting that there was sensory cortex on both sides of the tumor. Predictably, tumor removal produced a mild paresis of the left ankle and toe muscles, and sensory deficits in the corresponding area.

In 8 out of 12 patients, the MEG-EMG coherence maxima were located with a satisfactory goodness of fit of the single-dipole model. These results thus provided additional independent measure to confirm the central sulcus location.

The anatomical MRI landmarks yielded useful information in all patients. The omega-shaped knob of the precentral gyrus in the hand region was identified in 11 out of 12 affected hemispheres, and it agreed with functional localization in the operated patients. The ramus posterior of cingulate sulcus was useful as a landmark in 10 of 12 affected hemispheres. A wider precentral than postcentral gyrus was observed in 9 of 12 affected and in 10 of 12 non-affected hemispheres. The precentral and postcentral gyrus widths 3 mm lateral from the longitudinal fissure were, on average, 10 ± 5 mm and 7 ± 3 mm ($p < 0.02$) in the left hemisphere, and 11 ± 4 mm and 7 ± 3 mm ($p < 0.01$) in the right hemisphere. Postcentral gyrus was wider than precentral one in one left and in two right hemispheres and no difference was observed in one left and one right hemisphere.

The operating neurosurgeon considered vein overlay on 3-D MRIs to be very practical. The venograms

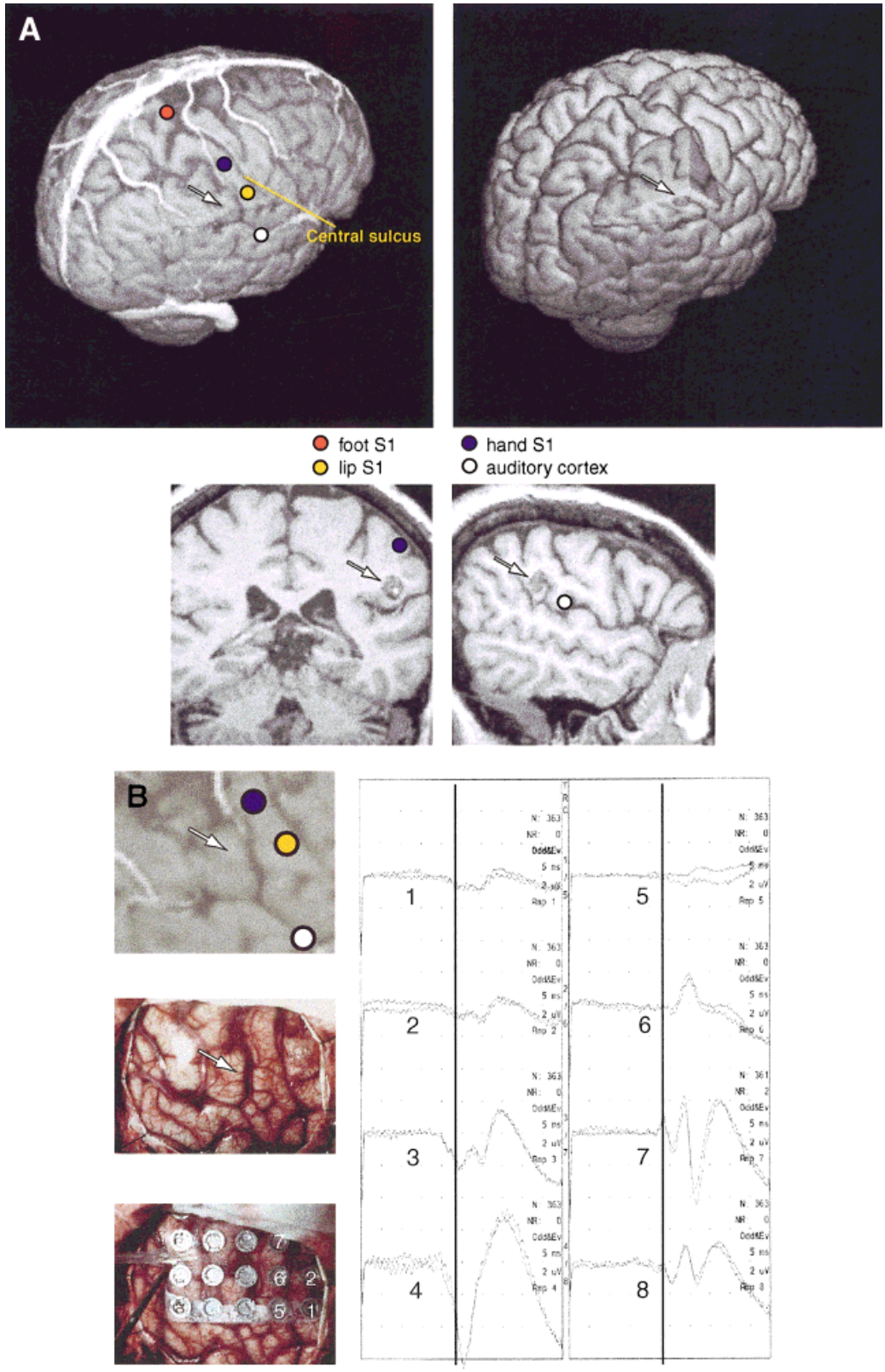

Figure 2.

A: Left, above: 3-D surface rendering of the brain of Patient 10, including cortical veins and sources of SEFs and AEFs. Right, above: Section of the 3-D surface rendering is removed to reveal the subcortical cavernous hemangioma, and the sulcal route used for its removal. Below: A coronal MRI section showing the source of median nerve SEF, and a sagittal section showing the source of AEF 100-ms response. The tumor is below the median nerve source and posterior to the AEF source; in combination with the sulcal pattern this finding pinpoints the tumor projection to the cortical surface, readily identified during the exposure of the cortex. The arrows show the approximate location of the subcortical tumor. **B:** Left, above: Enlarged section of the 3-D surface rendering of Patient 10. Intraoperative photograph without (middle) and with the SEP recording grid (below). Right: Intracortical SEPs from 8 electrodes. The electrode numbers are indicated on the grid; polarity reversal of SEP at 23 ms occurs between electrodes 3 and 7 (electrodes 3, 4, and 8 are under the dura). The arrows show the approximate location of the subcortical tumor.

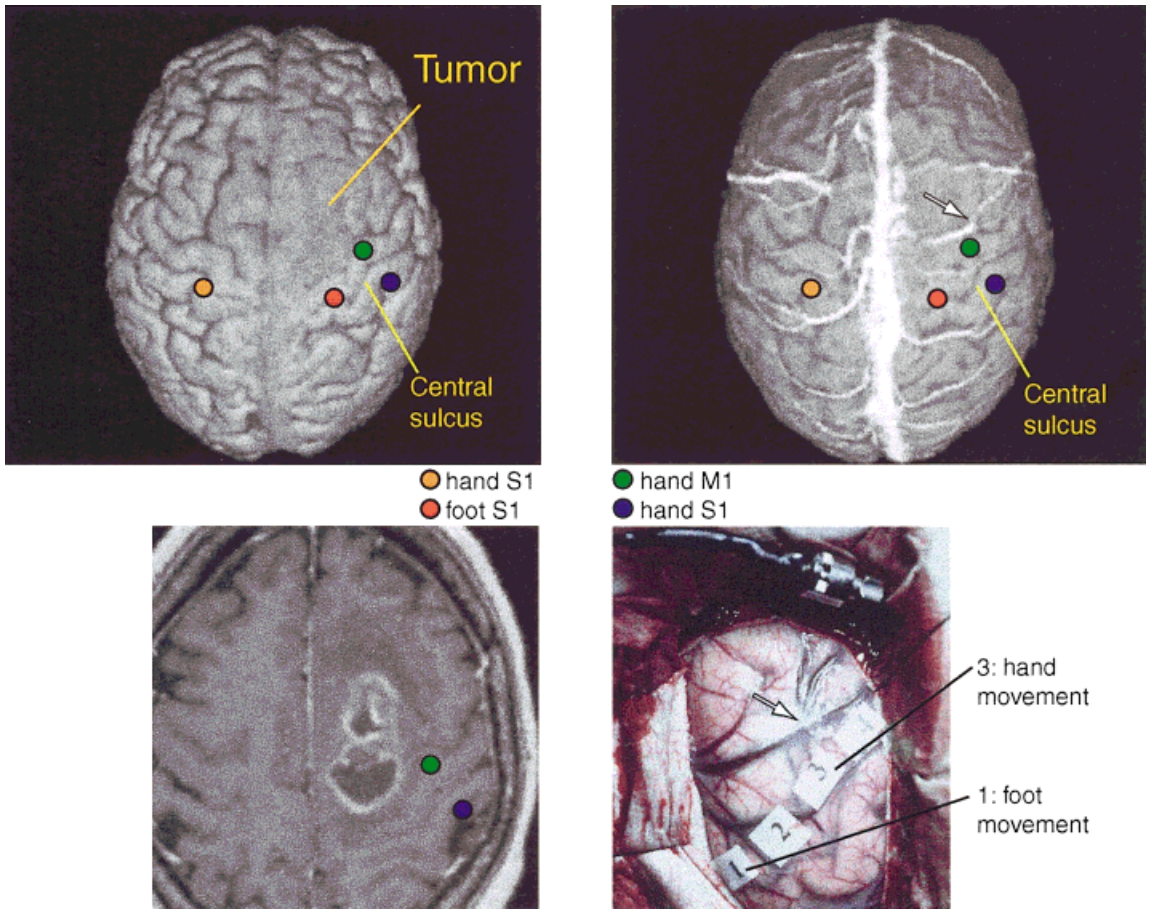

Figure 3.

Above: Preoperative 3-D surface renderings of the brain of Patient 12, without (left) and with (right) superimposed veins. Sources of responses to right median and left median and tibial nerve stimulation are overlaid on the surface rendering. Below, left: horizontal MRI section showing the tumor and sources of MEG-EMG coherence to left wrist extension, and SEFs to left median nerve stimulation. Below, right: Intraoperative photograph showing venous structure and stimulation sites used to define the motor cortex location. The arrow in the MR surface rendering and in the photograph point to the same vein. The distance between the source of maximum MEG-EMG coherence and stimulation site was 6 mm.

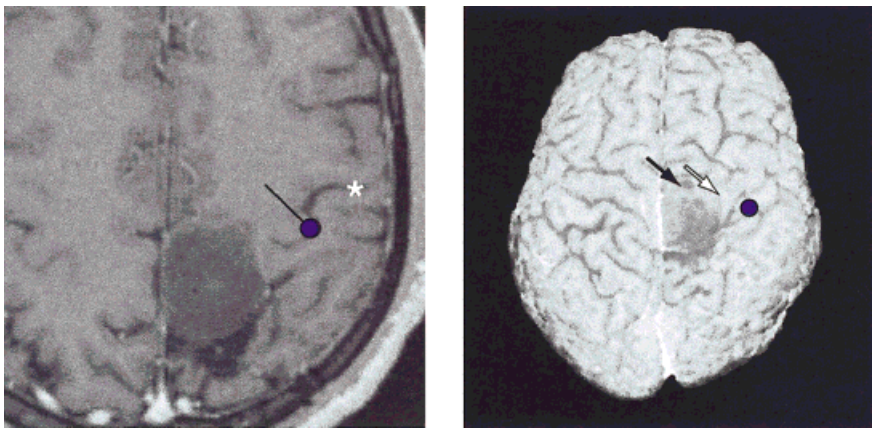

Figure 4.

Left: Source of the 20-ms SEF to median nerve stimulation overlaid on the horizontal MR slice of Patient 5 with a recurrent parasagittal astrocytoma GII on both sides of the central sulcus. The dot gives the location and the line the current orientation. Central sulcus is marked with an asterisk. The omega-shaped knob of the motor cortex is clearly visible. Right: N20m source to median nerve stimulation overlaid on the 3-D surface rendering of the patient. Responses to tibial nerve stimulation were absent. In intraoperative stimulation, the motor cortex was located anterior to the tumor; stimulation of the sites pointed by black and white arrows elicited weak foot and hand movenments, respectively.

were particularly helpful and clearly more useful than the sulcal pattern alone in identification of the tumor area and the putative eloquent cortex, to be verified by subsequent stimulation.

Patients 5, 7, 8, and 11 suffered from recurrent glioma, and ferromagnetic dust from the drilling in previous operations produced considerable noise to the signals. However, in all these four patients, the central sulcus was identified reliably by MN- and TN-SEFs. In Patient 11, who had strong slow-wave activity in the vicinity of the tumor, AEFs and LIP-SEFs were not analyzed further due to their low signal-to noise ratio.

DISCUSSION

Our preoperative MEG evaluation agreed well with intraoperative cortical stimulation and evoked potential recordings, in line with previous reports [Gallen, et al., 1993; Kamada, et al., 1993; Gallen, et al., 1995; Rezai, et al., 1996; Ganslandt et al., 1997; Hund et al., 1997; Nakasato et al., 1997]. The differences between preoperatively and intraoperatively evaluated cortical representations were well within the error limits of the methods applied. Because of methodological reasons, complete match between our pre- and intraoperative locations cannot be expected. For example, the SEF source location should correspond to the polarity inversion line of the SEP, not to the location of the electrode picking up the maximum signal which we used in our different measures. Furthermore, cortical stimulations were performed with a probe of 4-mm tip diameter under tags of 10×7 mm^2, and the optimal site of eliciting sensations was not searched.

One purpose of preoperative imaging is to help the surgeon to select the optimal approach to the tumor region. Preoperative imaging also provides information for the surgeon and the patient to decide the extent of tumor resection already before the operation, balancing the risk of damaging important functions against the remaining tumor volume. Naturally, intraoperative functional identification cannot be used for such purposes. The preoperative information also speeds up intraoperative stimulation and recordings because the most relevant brain areas for such procedures are already implicated. Intraoperative cortical stimulation may lengthen the operation when there is no preoperative data where to look for the eloquent cortex, and prolonged stimulation increases the risk of seizures. In a recent standardized preoperative evaluation of operative risks, based on the MEG source locations, the operation produced no residual symptoms when the distance between the tumor and the functional landmarks exceeded 6 mm [Hund, et al., 1997].

The success of our preoperative localization was based on combination of several methods: (1) SEFs were recorded to stimulation of 2–3 sites per body side, (2) MEG-EMG coherence was calculated for upper and lower extremities, (3) the knob in the motor cortex hand area was identified from the MRIs, (4) the widths of the precentral motor and postcentral somatosensory gyri were compared, and (5) the central sulcus was identified as the sulcus anterior to the posterior ramus of the cingulate sulcus in the mesial surface. All available anatomical landmarks agreed with functional localization. The precentral gyrus was generally wider than the postcentral one at the vertex. The omega-shaped knob of the central sulcus in the hand region proved to be especially useful; highlighting it in the 3-D MRIs (e.g., Kikinis et al., 1996) would probably provide a useful starting point for intraoperative search for motor cortex, even without additional functional information.

Eight of our 12 patients showed reliable MEG-EMG correlograms which confirmed the central sulcus location. Comparison of source locations of the MEG signals with maximum coherence with intracortical stimulations and recordings suggested origin of these MEG signals in the motor cortex, as has been previously suggested both in healthy humans [Conway, et al., 1995; Salenius, et al., 1997; Hari and Salenius, 1999], and in monkeys [Lemon, 1995]. This interpretation is at variance with the observed postcentral EEG-EMG coherence maximum in subdural EEG recordings of one epileptic patient [McLachlan and Leung, 1991]. However, the postcentral EEG maximum could reflect activity (tangential currents) in the anterior wall of the central sulcus, because the corticomotor projection originates mainly from the caudal part of the primary motor cortex [Lemon, 1995].

The MEG-EMG coherence may be especially useful in patients in whom SEFs cannot be elicited due to polyneuropathy or a lesion in the somatosensory cortex. One possible reason for the lack of MEG-EMG coherence in some patients may be the absence of 20-Hz rhythmicity in their motor cortex. The success rate for MEG-EMG coherence localization may be improved by methodological development, for instance by recording EMG during isometric tasks from several muscles, and by designing equipment assisting the patient to maintain steady force during the task.

Illustration of veins on the 3-D MRIs proved to be an extremely useful navigation tool for the neurosurgeon, clearly facilitating orientation to tumor in a limited field of exposed cortex. Consequently, the selection of appropriate sites for intracortical stimulation and for SEP grid positioning were speeded up, particularly in operations for recurrent gliomas where anat-

omy was blurred and dural adhesions complicated the surgery. Furthermore, the 3-D MRIs including functional landmarks and veins eased orientation to subcortical tumors when functional landmarks were in the vicinity of the tumor, and helped the surgeon to decide how to approach tumors from the surface (cf. Fig. 2). The vein overlay on the 3-D MRIs has been described previously [Kamada, et al., 1993; Gallen, et al., 1995], but has for some reason not obtained widespread clinical applications. The method can be recommended for all applications of functional identification in brain surgery. Functional data can easily be incorporated into intraoperative stereotaxic navigation methods [Rezai, et al., 1996; Ganslandt, et al., 1997]. The 3-D images with superimposed veins could alleviate the inaccuracy caused by possible brain shifts, due to, e.g., cyst evacuation, in conventional neuronavigation systems. The use of digital coordinate system instead of surface anatomy would naturally make comparison of preoperative and intraoperative localization more accurate.

The central sulcus can be identified preoperatively also by other methods. Functional MRI (fMRI) identifies the rolandic cortex by activation produced by tactile stimulation and motor tasks [Fried et al., 1995; Yousry et al., 1995; Atlas et al., 1996; Mueller et al., 1996]. fMRI yields useful preoperative information in about 80% of the patients [Pujol et al., 1998]. However, specific activation of motor or somatosensory cortex is not achieved, and the method is easily contaminated by motion artefacts [Krings et al., 1998]. The fMRI and MEG localization of the central sulcus in the same patients differed in about 20% of the affected hemispheres; the MEG localizations were confirmed by intraoperative SEP recordings [Inoue et al., 1999]. Dipole modelling of SEPs recorded from the scalp gave central sulcus location by about 1-cm accuracy in previously unoperated patients [Buchner et al., 1994; Mine et al., 1998]. However, changes in the conductivity due to oedema and tumor in the vicinity of the somatosensory cortex worsen the accuracy [Mine, et al., 1998], and the effects of skull breaches in operated patients have not been evaluated. Transcranial magnetic stimulation (TMS) can locate motor cortex in healthy subjects with 5–22 mm accuracy [Wasserman et al., 1996]; however, we are not aware of TMS's accuracy in neurosurgical patients. Positron emission tomography, combined with 3-D MRI allows, in addition to identification of sensorimotor regions, some evaluation of the extent of the glioma infiltration [Nariai et al., 1997], but requires a source and injections of radioactive isotopes. About 30% of PET studies fail to produce statistically significant activation by vibrotactile stimulation in the contralateral central region [Bittar et al., 1999]. Thus, MEG localization of sensorimotor regions compares favorably with results achieved by other methods.

CONCLUSIONS

Preoperative SEF recordings identified the central sulcus in all our patients. Intracortical stimulation and recordings confirmed that MEG signals coherent with EMG are generated in the motor cortex, and the use of the MEG-EMG coherence increased the reliability of motor strip identification. Display of veins on the 3-D renderings of the brain surface eased the use of preoperative information about sites of eloquent cortical areas during operation. MEG devices are becoming less costly and will in the near future be installed in many neuroradiological units, rendering the described methods more easily available. In the future, functional cortical localization, tailored individually for each patient, could be a standard procedure before surgical exposure for any brain pathology.

ACKNOWLEDGMENTS

This study has been supported by the Academy of Finland, and EU's Biotech programme. We thank Dr. V. Jousmäki for design and construction of the vibrotactile stimulator.

REFERENCES

Ahonen A, Hämäläinen M, Kajola M, Knuutila J, Laine P, Lounasmaa O, Parkkonen L, Simola J, Tesche C (1993): 122-channel SQUID instrument for investigating the magnetic signals from human brain. Physica Scripta T49:198–205.

Atlas S, Howard R, Maldjian J, Alsop D, Detre J, Listerud J, D'Esposito M, Judy K, Zager E, Stecker M (1996): Functional magnetic resonance imaging of regional brain activity in patients with intracerebral gliomas: findings and implications for clinical management. Neurosurg 38:329–338.

Baker S, Olivier E, Lemon N (1997): Coherent oscillations in monkey motor cortex and hand muscle EMG show task-dependent modulation. J Physiol 501:225–241.

Berger M, Cohen W, Ojemann G (1990): Correlation of motor cortex brain mapping data with magnetic resonance imaging. J Neurosurg 72: 383–387.

Bittar R, Olivier A, Sadikot A, Andermann F, Comeau R, Cyr M, Peters T, Reutens D (1999): Localization of somatosensory function by using positron emission tomography scanning; a comparison with intraoperative cortical stimulation. J Neurosurg 90:478–483.

Buchner H, Adams L, Knepper A, Rüger R, Laborde G, Gilsbach J, Ludwig I, Reul J, Scherg M (1994): Preoperative localization of the central sulcus by dipole source analysis of early somatosensory evoked potentials and three-dimensional magnetic resonance imaging. J Neurosurg 80:849–856.

Conway B, Halliday D, Farmer S, Shahani U, Maas P, Weir A, Rosenberg J (1995): Synchronization between motor cortex and spinal motoneuronal pool during the performance of a maintained motor task in man. J Physiol 489(3):917–924.

Fried I, Nenov V, Ojemann S, Woods R (1995): Functional MRI and PET imaging of rolandic and visual cortices for neurosurgical planning. J Neurosurg 83:854–861.

Gallen C, Schwartz B, Bucholz R (1995): Presurgical localization of functional cortex using magnetic source imaging. J Neurosurg 82:988–994.

Gallen C, Sobel D, Waltz T, Aung M, Copeland B, Schwartz B, Hirschkoff E, Bloom F (1993): Noninvasive presurgical mapping of somatosensory cortex. Neurosurg 33: 260–268.

Ganslandt O, Steinmeier R, Kober H, Vieth J, Kassubeck J, Romstöck J, Strauss C, Fahlbusch R (1997): Magnetic source imaging combined with image-guided frameless stereotaxy: a new method in surgery around the motor strip. Neurosurg 41:621–628.

Hämäläinen MS, Sarvas J (1989): Realistic conductivity geometry model of the human head for interpretation of neuromagnetic data. IEEE Trans Biomed Eng 36:165–171.

Hari R, Forss N. 1999. Magnetoencephalography in the study of human somatosensory cortical processing. Phil Trans R Soc Lond B 354:1145–1154.

Hari R, Salenius S (1999): Rhythmical corticomotor communication. NeuroReport 10: R1–R10.

Hund M, Rezai A, Kronberg E, Cappell J, Zoneshayn M, Ribary U, Kelly P, Llinas R (1997): Magnetoencephalographic mapping: basis of new functional risk profile in the selection of patients with cortical brain lesions. Neurosurg 40:936–943.

Inoue T, Shimizu H, Nakasato N, Kumabe T, Yoshimoto T (1999): Accuracy and limitation of functional magnetic resonance imaging for identification of the central sulcus: comparison with magnetoencephalography in patients with brain tumors. NeuroImage 10:738–748.

Kamada K, Takeuchi F, Kuriki S, Oshiro O, Houkin K, Abe H (1993): Functional neurosurgical simulation with brain surface magnetic resonance images and magnetoencephalography. Neurosurg 33:269–273.

Kikinis R, Gleason P, Moriarty T, Moore M, Alexander E, Stieg P, Matsumae M, Lorensen W, Black P, Jolesz F (1996): Computer-assisted interactive three-dimensional planning for neurosurgical procedures. Neurosurg 38:640–651.

Krings T, Reul J, Spetzger U, Klusmann A, Roessler F, Gilsbach J, Thron A (1998): Functional magnetic resonance mapping of sensorimotor cortex for image-guided neurosurgical intervention. Acta Neurochir 140:215–222.

Lemon R (1995): Cortical control of skilled movements. In: Cody F, editor. Neural control of skilled human movement. London: Portland Press, p 1–11.

McLachlan R, Leung L (1991): A movement-associated fast rolandic rhythm. J Can Neurol Sci 18:333–336.

Mine S, Oka N, Yamaura A, Nakajima Y (1998): Presurgical functional localization of primary somatosensory cortex by dipole tracing method of scalp-skull-brain head model applied to somatosensory evoked potential. Electroenceph clin Neurophysiol 108:226–233.

Mueller W, Yetkin F, Hammeke T, Morris G, Swanson S, Reichert K, Cox R, Haughton V (1996): Functional magnetic resonance imaging mapping of the motor cortex in patients with cerebral tumors. Neurosurg 39:515–521.

Nakasato N, Kumabe T, Kanno A, Ohtomo S, Mizoi K, Yoshimoto T (1997): Neuromagnetic evaluation of cortical auditory function in patients with temporal lobe tumors. J Neurosurg 86:610–618.

Nariai T, Senda M, Ishii K, Maehara T, Wakabayashi S, Toyama H, Ishiwata K, Hirakawa K (1997): Three-dimensional imaging of cortical structure, function and glioma for tumor research. Nucl Med 38:1563–1568.

Pujol J, Conesa G, Deus J, Lopez-Obarrio L, Isamat F, Capdevila A (1998): Clinical application of functional magnetic resonance imaging in presurgical identification of the central sulcus. J Neurosurg 88:863–869.

Rezai A, Hund M, Kronberg E, Zoneshayn M, Cappell J, Ribary U, Kall B, Llinas R, Kelly P (1996): The interactive use of magnetoencephalography in stereotactic image-guided neurosurgery. Neurosurg 39:92–102.

Rosenberg J, Amjad A, Breeze P, Brillinger D, Halliday D (1989): The fourier approach to the identification of functional coupling between neuronal spike trains. Prog Biophys Molec Biol 53:1–31.

Salenius S, Portin K, Kajola M, Salmelin R, Hari R (1997): Cortical control of human motoneuron firing during isometric contractions. J Neurophysiol 77:3401–3405.

Skirboll S, Ojemann G, Berger M, Lettich E, HR W (1996): Functional cortex and subcortical white matter located within gliomas. Neurosurg 38:678–685.

Sutherling W, Crandall P, Darcey T, Becker D, Levesque M, Barth D (1988): The magnetic and electric fields agree with intracranial localizations of somatosensory cortex. Neurol 38:1705–1714.

Wasserman E, Wang B, Zeffiro T, Sadato N, Pascual-Leone A, Toro C, Hallett M (1996): Locating the motor cortex on the MRI with transcranial magnetic stimulation and PET. NeuroImage 3:1–9.

Wood C, Spencer D, Allison T, McCarthy G, Williamson P, Goff W (1988): Localization of human sensorimotor cortex during surgery by cortical surface recording of somatosensory evoked potentials. J Neurosurg 68:99–111.

Wunderlich G, Knorr U, Herzog H, Kiwit J, Freund H-J, Seitz R (1998): Precentral glioma localization determines the displacement of cortical hand representation. Neurosurg 42:18–27.

Yousry T, Schmid U, Alkadhi H, Schmidt D, Peraud A, Buettner A, Winkler P (1997): Localization of the motor hand area to a knob on the precentral gyrus. A new landmark. Brain 120:141–157.

Yousry T, Schmid U, Jassoy A, Schmidt D, Eisner W, Reulen H-J, Reiser M, Lissner J (1995): Topography of the cortical motor hand area: prospective study with functional MRI imaging and direct motor mapping at surgery. Radiol 195:23–29.